RSC Advances

PAPER

View Article Online
View Journal | View Issue

Cite this: *RSC Adv.*, 2020, **10**, 1181

Bi_2O_3 and g-C_3N_4 quantum dot modified anatase TiO_2 heterojunction system for degradation of dyes under sunlight irradiation

Weidong Peng,[ab] Chun Yang[cd] and Jiang Yu *[ab]

Received 15th September 2019
Accepted 9th December 2019

DOI: 10.1039/c9ra07424d

rsc.li/rsc-advances

A facile and feasible method was successfully utilized to incorporate Bi_2O_3 and g-C_3N_4 quantum dots on TiO_2 surface to synthesize a novel composite g-C_3N_4/TiO_2/Bi_2O_3. The photocatalytic activity of the composite g-C_3N_4/TiO_2/Bi_2O_3 for degradation of dyes under sunlight and UV light irradiation was evaluated. It possessed the higher photocatalytic performance than that of pristine TiO_2 or g-C_3N_4 under the same conditions. Under sunlight irradiation, the reaction rate constants of the g-C_3N_4/TiO_2/Bi_2O_3 was about 4.2 times and 3.3 times higher than that of TiO_2 and g-C_3N_4, respectively. The promising photocatalytic performance was attributed to the broader light absorption range and efficient separation of photoinduced carriers. Moreover, based on the TEM, XPS, XRD, UV-vis spectrum, radicals scavenging test and Mott–Schottky analysis systematic mechanism for photodegradation process was proposed. This work provides a promising strategy for the modification of TiO_2-based semiconductors by incorporating different quantum dots and promoting the efficiency of the photocatalysts in practical application.

1 Introduction

At present, environmental contamination and energy shortage are the most serious problems on our planet. Hence, there is an urgent need for the development of an environmental, sustainable, economical and energy-saving technology for contamination control. Semiconductor photocatalysis provides an optimal solution for the problems with the potential that the clean solar energy can be harnessed for decomposition of pollutants.[1] To date, TiO_2 as the photocatalyst has drawn significant attention and been widely studied because of its desirable properties including high reactivity, chemical stability, nontoxicity, and cheap price.[2–7] Nevertheless, the application of TiO_2-based photocatalysts is hindered due to its inefficient utilization of solar energy, poor charge separation, and low adsorption of organic contaminants on the surface. Besides these intrinsic drawbacks, the complicated process of synthesis is another key factor to impede its practical application.[8]

To avoid the above limitation, various modification strategies have been carried out, such as dye-sensitization, metal or non-metal doping, and transition metal doping, *etc.* Particularly, compositing TiO_2 with different semiconductor into heterojunction is an efficient method to enhance the photocatalytic activity.[8] Since the heterojunction structure would decrease the recombination of electron/hole by separating the charge carriers to different semiconductors surface due to the different potential barriers. These heterojunctions-based semiconductors exhibit advanced efficiency for degrading pollutants.

Presently, considerable attention has been paid to graphitic carbon nitride (g-C_3N_4), which is a stable kind of polymers with a layered structure like graphene. Particularly, it possesses the strong ability to harvest solar energy due to its narrow band gap (E_g = 2.7 eV). Nevertheless, the quantum efficiency of pure g-C_3N_4 is low because of the high recombination ratio of photogenerated electron/hole pair.[9] Combining the TiO_2 with g-C_3N_4 in heterojunction is considered as an efficient method which can improve the absorption of visible light and the separation of photogenerated pairs. Yu *et al.*[10] synthesized g-C_3N_4–TiO_2 composites by calcination process using P25 and urea, achieving the high photoactivity for the degradation of HCHO. Lei *et al.*[11] reported the synthesis of g-C_3N_4/TiO_2 photocatalyst *via* simple calcination using cyanamide and anatase TiO_2 as precursor. The g-C_3N_4/TiO_2 photocatalyst exhibits a promising progress in degradation of the dye Acid Orange 7 under both visible and UV light. The g-C_3N_4–TiO_2 composites with prominent photoactivity for the degradation of phenol under UV light

[a]College of Architecture and Environment, Sichuan University, Chengdu, 610065 China. E-mail: yuj@scu.edu.cn
[b]Institute of New Energy and Low Carbon Technology, Sichuan University, Chengdu, 610065 China
[c]College of Chemistry and Materials Science, Sichuan Normal University, Chengdu, 610068 China
[d]Computational Visualization and Virtual Reality Key Laboratory of Sichuan Province, Chengdu 610068, China

was synthesized by Colo'n *et al.*[12] by impregnation. Zhang *et al.*[13] found that well-dispersed TiO_2 nanocrystals with (001) facets prepared *in situ* on g-C_3N_4 through a solvothermal method exhibit higher efficiency for photocatalytic degradation of phenol as compared to pure g-C_3N_4 and TiO_2. Wu *et al.*[14] prepared nanosheets TiO_2/g-C_3N_4 composite by solvothermal method, which exhibits a significant improvement in photodegradation towards methylene blue under visible light irradiation than pristine g-C_3N_4 and TiO_2.

Among strategies of constructing heterojunction, synthesis of p–n junction is considered as an effective method to facilitate the photoactivity by inducing the separation of photogenerated carries due to the existence of an internal electric field. Bismuth oxide (Bi_2O_3), as a p-type semiconductor, has been extensively studied due to its suitable band gap ($E_g = 2.8$ eV) and visible light driven catalytic activity. Among the six different polymorphic phases of Bi_2O_3, β-Bi_2O_3 has prominent advantages for degradation of pollutants. Since TiO_2 is a n-type semiconductor, it is feasible to combine TiO_2 with β-Bi_2O_3, by which catalytic efficiency can be notably enhanced.[15–18] Recently, much efforts have been made to synthesize TiO_2/Bi_2O_3 heterojunction. Various methods have been employed such as: pulse electrodeposition,[19] hydrothermal, sol–gel, and coprecipitation.[20–26] However, the complexity of these methods limits the application of photocatalysis.

Instead of above strategies, researchers have succeeded in sensitizing TiO_2 by modifying quantum dots (QDs) of low-band gap materials such as g-C_3N_4, CdS, CdSe, CdTe, and Bi-based materials, which can absorb light in the visible region. QDs can match the solar spectrum better due to the particle size effect. Additionally, QDs are recently reported to generate multiple excitons, which can improve the photocatalysis efficiency.[27–30] Jiao *et al.*[31] firstly prepared Bi_2O_3 quantum dots decorated TiO_2 with exposed {001} facets on graphene sheets. Size-controllable were *in situ* synthesized on TiO_2 nanotube arrays and high activity in synergetic H_2 evolution and organics degradation.[32]

In this study, we firstly use a simple ball-milling/calcination method to synthesize a g-C_3N_4/TiO_2/Bi_2O_3 heterojunction system which distinctly exhibit a promising synergetic improvement effect. The different properties of the catalyst are evaluated by the degradation of simulated dyeing wastewater under UV light and direct sunlight irradiation. While the different properties are confirmed by TEM, XPS, XRD and UV-vis diffuse reflection spectra. A tentative mechanism for photocatalytic degradation of RhB by the composite g-C_3N_4/TiO_2/Bi_2O_3 is proposed.

2 Materials and methods

2.1 Catalysts synthesis

2.1.1. Chemicals and reagents. Double distilled water was used throughout the experiment. The catalyst precursor used in this experiment including titanium dioxide (TiO_2, anatase, 99.8%; Shanghai Aladdin Biochemical Technology Co., Ltd), melamine (98%; Shanghai Aladdin Biochemical Technology Co., Ltd), bismuth(III) nitrate-pentahydrate ($Bi(NO_3)_3 \cdot 5H_2O$, 98%; Shanghai Aladdin Biochemical Technology Co., Ltd). All the reagents utilized were of analytical grade and without further purification.

2.1.2 Methods

1. *Synthesis of pure g-C_3N_4.* 5 g of melamine were added into crucible with a cover then heated at 520 °C under air atmosphere for 2 h with a heating rate of 5 °C min^{-1}. After cooling to the room temperature naturally, the resulting yellow bulks were collected and ball-milled into powders for further evaluation.

2. *Synthesis of pure Bi_2O_3.* 3 g $Bi(NO_3)_3 \cdot 5H_2O$ were added into crucible with a cover then heated at 520 °C under air atmosphere for 2 h with a heating rate of 5 °C min^{-1}. After cooling to the room temperature naturally, the resulting bulks were collected and ball-milled into powders for further evaluation.

3. *Synthesis of g-C_3N_4/TiO_2/Bi_2O_3.* The g-C_3N_4/TiO_2/Bi_2O_3 catalysts were prepared by the processes of ball-milling and calcination. Firstly, 400 mg of anatase TiO_2 powders and 600 mg of melamine were added into the agate ball milling tank, followed by the process of ball milling for 2 h with a ball powder ratio of 10 : 1, at a speed of 400 rpm in a planetary ball mill. Then, a certain amount of $Bi(NO_3)_3 \cdot 5H_2O$ were added into the agate ball milling tank which was filled with TiO_2 and melamine. The powders mixed by ball milling for 2 h with a ball powder ratio of 10 : 1, at a speed of 400 rpm in a planetary ball mill. Subsequently, the mixed powder was placed into a crucible with a cover then heated at 520 °C under air atmosphere for 2 h with a heating rate of 5 °C min^{-1}. After cooling to the room temperature naturally, the resulting yellow bulks were collected and ball-milled into powders for further evaluation. The obtained powers was named as TCB-*x*, where the *x* refers to the weight percentage of $Bi(NO_3)_3 \cdot 5H_2O$ to the weight of TiO_2 and melamine.

2.2 Characterization

The crystal phases was characterized by X-ray diffraction (XRD, Bruker D8 ADVANCE A25X) with a Cu Kα radiation with a diffraction angle between 10–80°

Transmission electron microscopy (TEM) and high-resolution transmission electron microscopy (HRTEM) were measured by Tecnai G2 F20 S-TWIN (200 kV). The samples were dispersed in ethanol and dropped on copper grids. Chemical composition and valence band (VB) were observed by X-ray photoelectron spectroscopy (XPS, Escalab 250Xi) using a monochromatic microfocused Al Kα (1486. 6 eV) source. UV-vis diffuse reflectance spectroscopy (UV-vis DRS) absorption spectra of the wavelength between 200 nm and 800 nm were carried out at a Shimadzu UV-3600 spectrophotometer using $BaSO_4$ as a reference.

The electrochemical studies were conducted on an electrochemical workstation (CHI660C, CH Instrument Corp, Shanghai), which used catalyst-deposited FTO glass as working electrode, Pt as the counter electrode and Ag/AgCl as the reference electrode. Meanwhile, 0.5 M Na_2SO_4 was served as the electrolyte solution. The working electrode was prepared as follows: 20 mg PEG-600 and 10 mg pure TiO_2 and Bi_2O_3 were dispersed in 1 mL ethanol and ultrasonically scattered for 1 h. Then, the suspension above was added onto the FTO glass (1 × 1 cm) and evaporated to dry. The Mott–Schottky measurement was performed at frequency of 1000 Hz.

2.3 Photocatalytic activity test

The aqueous Rhodamine B (RhB), methylene blue (MB) and methyl orange (MO) dyes were used as model organic contaminants to evaluate the photocatalytic activities of the synthesized catalysts. Degradation experiments were carried out under UV and direct solar light irradiation. A high-pressure 300 W mercury lamp with the radiation of 365 nm was used as the UV light source. To study the photocatalytic activity of the samples under visible light, the photoreactor were directly exposed to sunlight. And the illumination intensity was measured by solar power meter (TES-1333R). 50 mg catalyst powders were suspended in 50 mL aqueous organic dye solution and the dyes concentration was 20 mg L^{-1}. To reach adsorption–desorption equilibrium, the solution was stirred for 60 min in the dark. At given time intervals, 4 mL aliquots were taken and centrifuged at 10 000 rpm for 10 min to remove the particles. Then, the concentration of organic dyes in filtrates was analyzed using an Alpha-1506 UV-vis spectroscopy (Shanghai Lab-Spectrum Instruments Co. Ltd, China) at the wavelength of 554 nm, 664 nm, 465 nm for RhB, MB, MO, respectively. The experiments were repeated 3 times.

3 Result and discussion

3.1 XRD characterization

Fig. 1 shows the XRD patterns of TCB-30%, pristine TiO_2, g-C_3N_4 and Bi_2O_3. In TCB-30% patterns, the diffraction peaks at 25.3°, 37.9°, 48.0°, 53.9° could be well indexed to the (101), (004), (200) and (105) planes of the anatase phase TiO_2.[23,33] There are four peaks at 27.9°, 31.8°, 32.8°, 46.3°, corresponding to the (211), (002), (220), and (222) plane of pristine Bi_2O_3.[26,34,35] The characteristic peaks of g-C_3N_4 at 27.5° (ref. 27 and 36) was also detected in TCB-30% patterns. The diffraction peaks with relatively low intensity indicated the small sized Bi_2O_3 and TiO_2 quantum dots, in consistent with the results of TEM. The well crystallized diffraction peaks detected in TCB-30% patterns suggested the well crystalline structure of anatase TiO_2, g-C_3N_4 and Bi_2O_3, without the generation of other crystal structure.

3.2 Microstructure analysis

The morphology of the prepared catalysts was characterized by TEM and high-resolution. TEM image Fig. 2b, c and d are enlarged views of Fig. 2a. As shown in Fig. 2a, TiO_2 particles have a spherical structure with an average size between 30–60 nm, which was in well accordance with the crystallite size obtained from Scherrer equation. Bi_2O_3 and g-C_3N_4 showed a much smaller size below 10 nm, and intimately cover on the surface of TiO_2 particles, which intensively increase the specific surface area of TiO_2.

Clear lattice fringes for the identification of crystallographic spacing could be observed in Fig. 2c, and the lattice spacing of 0.350 nm and 0.321 nm corresponded well with (101) phase of TiO_2 and (221) phase of Bi_2O_3,[15–17] respectively. In Fig. 2d, the lattice spacing of 0.318 nm matched the (002) crystal phase of g-C_3N_4.[37–39]

Thus, these TEM images indicated the interaction of g-C_3N_4/TiO_2/TiO_2 heterojunction composite. The g-C_3N_4 and Bi_2O_3 located on the surface of TiO_2 as quantum dots. In Fig. 2e, the pure g-C_3N_4 showed aggregated morphologies, which were comprised of block-based flakiness. Fig. 2f displayed a spheroidal structure of Bi_2O_3. It was obvious that the process of ball-milling played a significant role in synthesizing g-C_3N_4 and Bi_2O_3 quantum dots on TiO_2 surface.

3.3 Chemical compositions

Fig. 3 showed the full survey and high-resolution spectra for the Ti 2p, O 1s, C 1s, N 1s and Bi 4f region. Fig. 3b depicts the C 1s of the prepared. The peak centered at 284.6 eV could be assigned to the adventitious carbon while the peak at 287.5 eV belongs to the N–C=N group of the g-C_3N_4.[40–42] Fig. 3d showed N 1s spectrum of catalyst. The N 1s peak was fitted into two peaks at 399.3 eV and 400.2 eV, which were the sp^2-hybridized nitrogen (C=N–C) and tertiary nitrogen (N-3), respectively.[40–42] Furthermore, two fitted peaks of Ti 2p3/2 and Ti 2p1/2 at 458.9 eV and 464.4 eV suggested the presence of Ti(IV).[27,36,43] In Fig. 3a, two fitted peaks at 158.9 eV and 164.3 eV belonged to Bi 4f5/2 and Bi 4f7/2, suggesting the existence of Bi_2O_3 in the catalyst.[24,34,35] These results suggested that the composite TCB-30% consisted of g-C_3N_4, anatase TiO_2 and Bi_2O_3.

3.4 UV-vis DRS analyses

The UV-vis diffuse reflectance spectra of different composites were exhibited in Fig. 4. It is obvious that the composite of TCB-30% showed a significant red shift of band edge to 456.5 nm compared with the initial TiO_2, Bi_2O_3 and g-C_3N_4. There is also an intensively long tailing absorption in visible region, which can be explained by the synergistic effects of Bi_2O_3 and g-C_3N_4 quantum dots with a narrower band gap.

The band gap energies were determined using the equation below:

$$\alpha h\nu = A(h\nu - E_g)^{n/2}$$

where A, h, ν, E_g and α are the absorption coefficient, Planck's constant, frequency, band gap energy and a constant, respectively. For the composites in this study, n is 4 because of the indirect transition. Therefore, Tauc's plots of $(\alpha h\nu)^{1/2}$ *versus* photon energy ($h\nu$) are obtained. As shown in Fig. 4b, the band gap energies of TiO_2, TCB-30%, Bi_2O_3 and g-C_3N_4 are 3.20 eV, 2.24 eV, 2.80 eV and 2.7 eV, respectively. The TCB-30% has a lower band gap energy compared to TiO_2, which may be due to the heterojunction structure of the composite.

In order to further explain the photocatalytic activity of the ternary composite, the band structure of Bi_2O_3 was explored according to the following empirical equation.

$$E_{CB} = X - E^e - 0.5E_g$$

$$E_{CB} = E_{VB} - E_g$$

where E_{VB} is the valence band edge potentials, E_{CB} is the conduction band energy, X is the electronegativity of

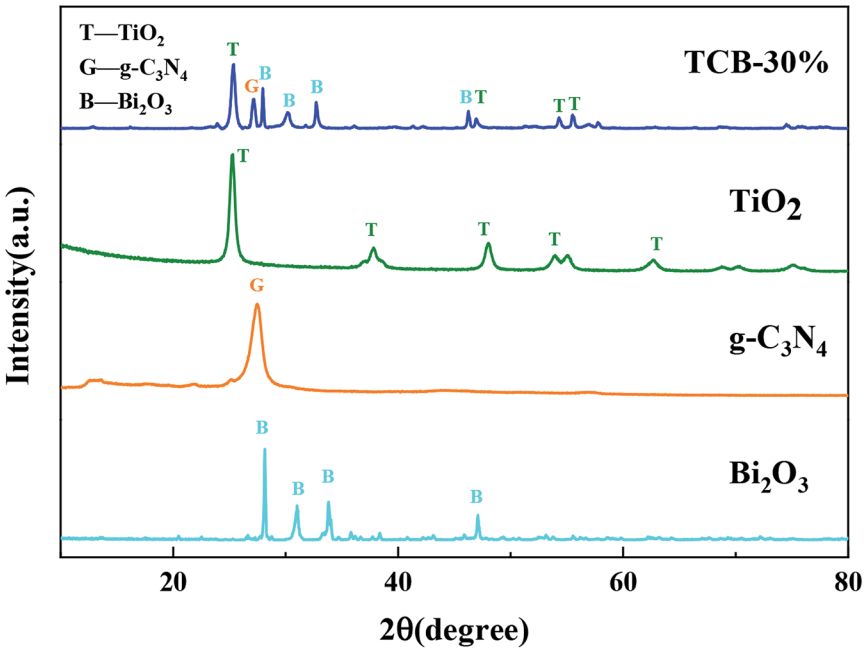

Fig. 1 XRD pattern of TCB-30%, TiO_2, g-C_3N_4 and Bi_2O_3.

semiconductor, E^e is the energy value of free electrons on the hydrogen scale, E_g is gap energy of semiconductor. The value of X for Bi_2O_3 is *ca.* 5.99 eV. The calculated conduction band and valence band of Bi_2O_3 are 0.33 eV and 3.13 eV, respectively. The band structure of TiO_2 and g-C_3N_4 was calculated in above-mentioned method as well. And the results were showed in Table 1.

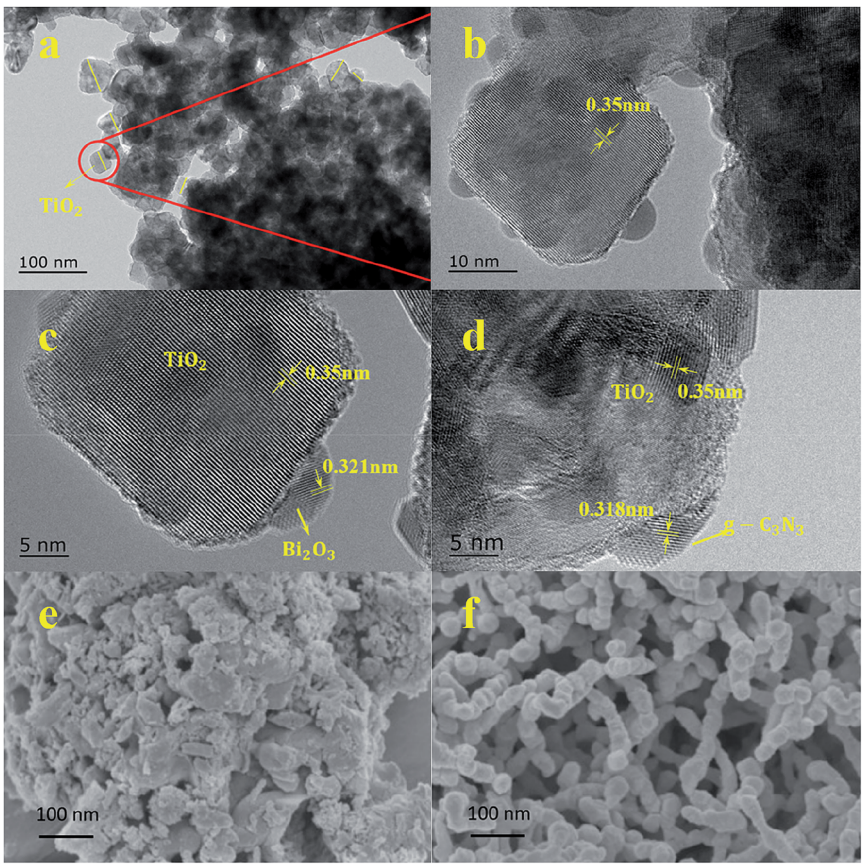

Fig. 2 (a) Selected TEM figure of TCB-30%, (b, c and d) HRTEM figures of TCB-30%, (e) SEM figure of pure g-C_3N_4, (f) SEM figure of pure Bi_2O_3.

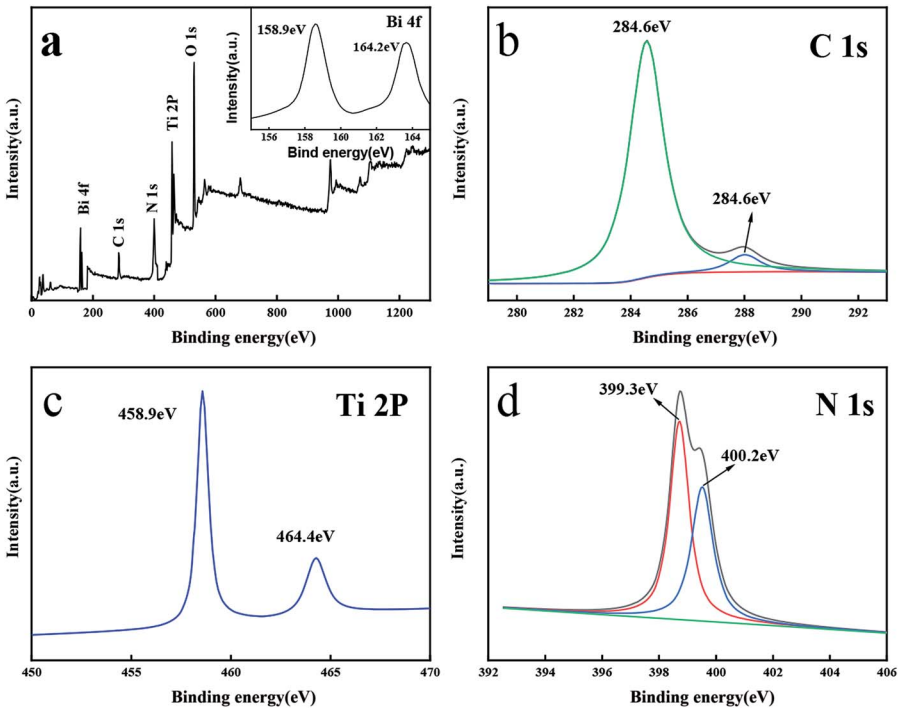

Fig. 3 XPS spectrum of (a) TCB-30%, (b) C 1s, (c) Ti 2P, (d) N 1s.

3.5 Photocatalytic activity

Fig. 5 displays the change of RhB concentration *versus* irradiation time with the pure TiO_2, g-C_3N_4 or TCB-*x* under UV irradiation and sunlight irradiation. From Fig. 5a, pure TiO_2 and pure g-C_3N_4 exhibited limited degradation rate of RhB under the UV light, which were only 66.9% and 62.1% after 50 min irradiation respectively. With the incorporation of Bi_2O_3 and construction of heterojunction, the photocatalytic activity substantially enhanced. In particular, the TCB-30% displayed the highest degradation rate of 96.5%. Moreover, TCB-30% showed the best photodegradation ability on RhB (completely degraded within 120 min) under sunlight irradiation (about 640 W m^{-2}).

The degradation of RhB followed the first-order kinetics, which can be expressed by the equation: $\ln(C_0/C_t) = k_a^{-1}t$, where C_0 and C_t is RhB concentration at time 0 and time t, and k_a^{-1} represents the first-order reaction rate constant. As shown in Fig. 6, TCB-30% displayed a maximum value of rate constant under UV, which was about 2.2 times as high as that of TiO_2 and 2.6 times as that of g-C_3N_4. When under the solar irradiation (640 W m^{-2}), the k_a^{-1} of TCB-30% was 4.2 times and 3.3 times higher than that of TiO_2 and g-C_3N_4 respectively. Therefore, the improvement of photocatalytic activity under solar irradiation is more remarkable than that in the condition of UV light.

Moreover, TCB-30% was also used to degrade different kinds of dyes with the same initial concentration under sunlight irradiation, including methylene blue (MB) and methyl orange

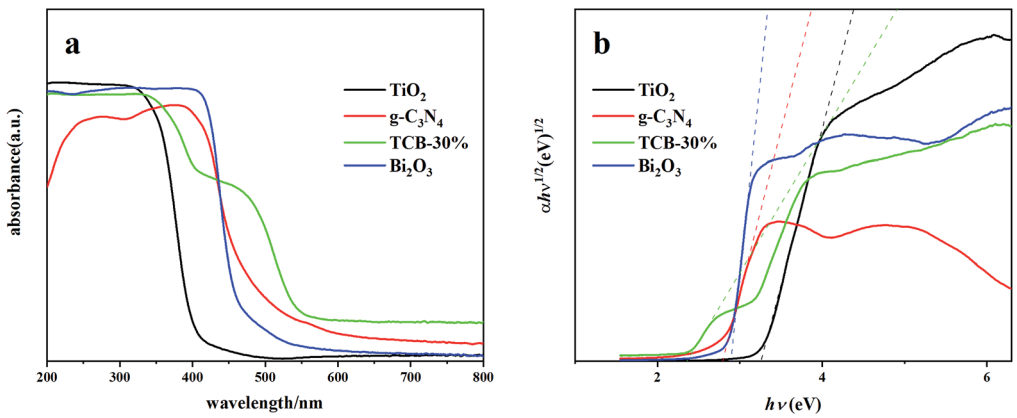

Fig. 4 (a) UV-vis DRS spectra and (b) optical bandgap of the TCB-30%, TiO_2, g-C_3N_4 and Bi_2O_3.

Table 1 Band structure of Bi_2O_3, TiO_2 and g-C_3N_4

Catalyst	Band gap (eV)	Valence band (VB)	Conduction band (CB)
TiO_2	3.2	2.7	−0.5
g-C_3N_4	2.7	1.4	−1.3
TCB-30%	2.2		
Bi_2O_3	2.8	3.13	0.33

(MO). As it shown in Fig. 7a, TCB-30% displayed a limited degradation rate for methylene blue and methyl orange compared with RhB. Fig. 8 showed the dark adsorption of three dyes over TCB-30%. It was supposed that the promising reaction rate could be contributed by the strong adsorption of the prepared heterojunction materials towards organic dyes with hydroxy groups. Thus, it is worth further research on how the surface groups of this composite affects the reaction with organic pollutants.

To figure out the contribution of photo-induced active radical in the reaction process, benzoquinone (BQ), isopropanol (IPA) and ammonium oxalate (AO) were applied as scavengers of superoxide radical ($\cdot O_2^-$), hydroxyl radical ($\cdot OH$) and hole (h^+), respectively. The comparison experiments were carried out in the presence of the same molar concentration of scavengers (BQ, IPA and AO) for visible light degradation of RhB with TCB-30%. As displayed in Fig. 9, the degradation rate without any scavengers is 99.6%. By contrast, by adding BQ and IPA, the degradation rate sharply suppressed. While with the addition of AO scavengers, there is only a slight decrease of degradation rate. Therefore, it can be concluded that superoxide radical ($\cdot O_2^-$) and hydroxyl radical ($\cdot OH$) play key roles in degradation towards RhB under visible light.

During the practical application of catalysts, the by-products tend to be adsorbed on the active sites of photocatalysts' surface, leading to the dramatic decrease of the photocatalytic activity. To evaluate the stability of the prepared TCB-30%, recycle experiments were conducted under solar irradiation. As shown in the Fig. 9, the TCB-30% still presents the excellent photocatalytic performance after three cycles.

3.6 Mechanism discussion

In order to investigate the electrochemical properties of TiO_2 and Bi_2O_3, Mott–Schottky plots were obtained. In Fig. 10a, TiO_2 exhibit a positive slope indicating that it's n-type semiconductor. On the contrary, BiO_2 shows a negative slope, which indicts a p-type semiconductor.

Based on the results of XRD, XPS, TEM and UV-vis DRS analysis and Mott–Schottky, a tentative heterojunction system proposed and depicted in Scheme 1. TiO_2 is placed as a support and connector of Bi_2O_3 and g-C_3N_4 quantum dots. The promising photocatalytic performance of TCB-30% under visible light is significantly related to the extended light adsorption spectrum and enhanced electron–hole separation.

On the one hand, the generation of g-C_3N_4 and Bi_2O_3 quantum dots with a narrow band gap facilitated the improvement of visible light harvesting ability, which motivates the generation of photoinduced carriers under visible light. On the

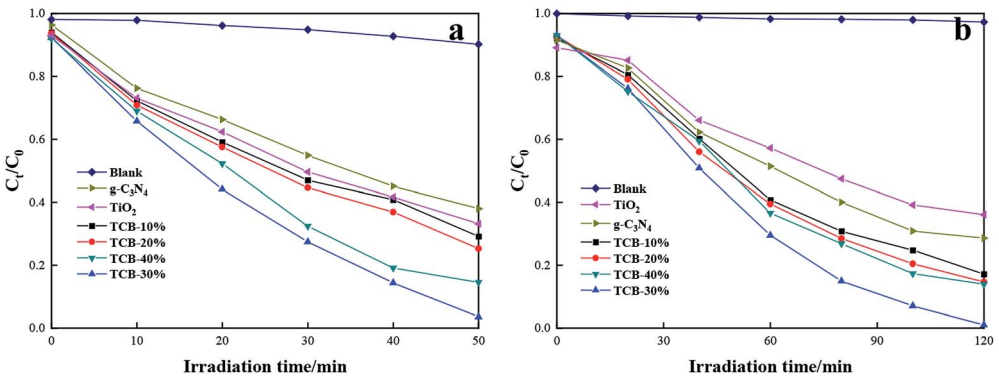

Fig. 5 Photocatalytic activity of TCB-30%, TiO_2 and g-C_3N_4 for degradation of RhB under (a) UV light irradiation (b) sunlight irradiation.

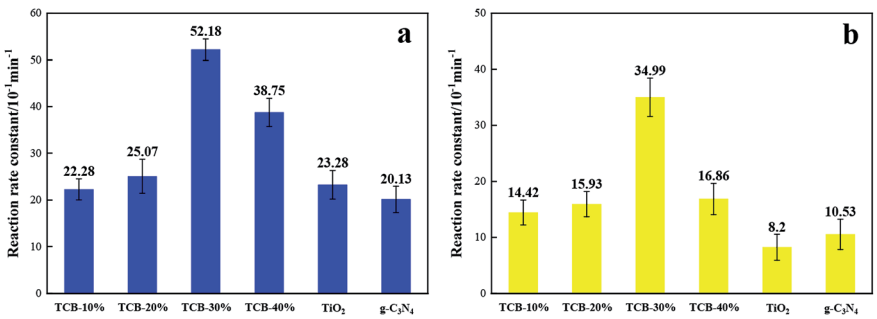

Fig. 6 Reaction rate constant for degradation RhB of TCB-30%, TiO_2, g-C_3N_4 and Bi_2O_3 under (a) UV light irradiation (b) sunlight irradiation.

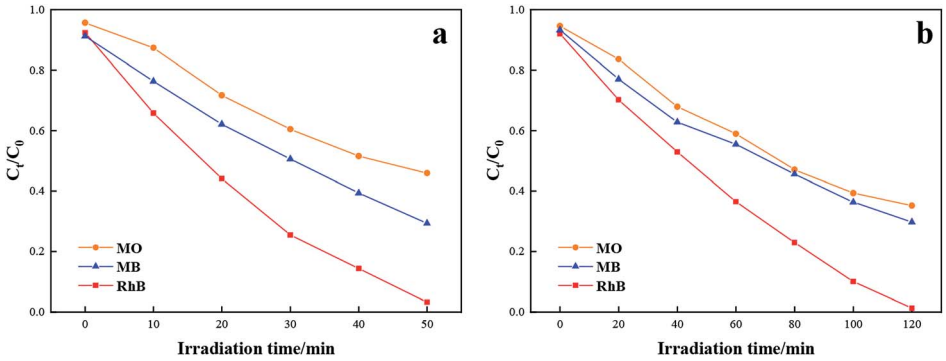

Fig. 7 Comparison of the photocatalytic activity towards degradation of RhB, MB and MO under (a) UV light irradiation (b) sunlight irradiation.

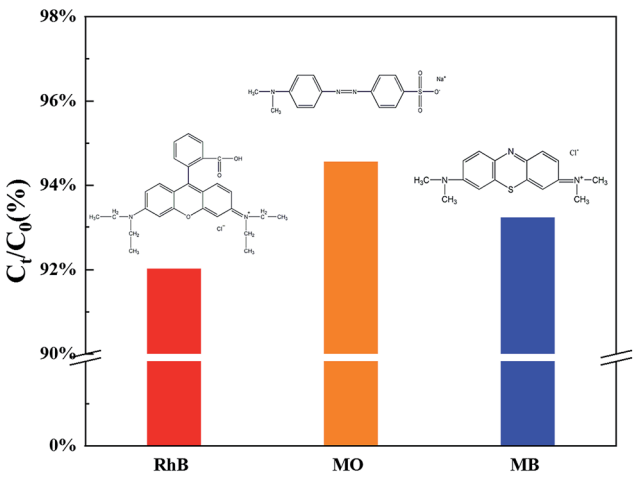

Fig. 8 Dark adsorption of three dyes over TCB-30%.

other hand, the Fermi energy level of n-type semiconductors located nearer to the VB while the Fermi energy of p-type semiconductors located nearer to the VB.[23,27,35] Therefore, after p-type Bi_2O_3 and n-type TiO_2 were in contact, the electrons near the interface diffused from TiO_2 to Bi_2O_3 while the holes diffused from Bi_2O_3 to TiO_2. When the electrons migrated from TiO_2, leaving a positively charged donor ion, and a positive charge region was formed on the side of the n region. In the same way, a negative charge region was formed on the side of p region. Therefore, there was no electrical neutrality on both sides of the interface of the p–n junction, and a positively and negatively charged region appeared, becoming a space charge region, which can force photoinduced electrons and holes to transfer in the opposite direction (Fig. 10b). The photogenerated electrons can only transfer from the CB of Bi_2O_3 to CB of TiO_2, in contrast the holes can only transfer from the VB of TiO_2 to the VB of Bi_2O_3, leading to a notably efficient separation of photoinduced pairs between Bi_2O_3 and TiO_2. As for the heterojunction between g-C_3N_4 quantum dots and TiO_2 particles, since the g-C_3N_4 has a more positive conduction band edge potential than that of TiO_2 (−0.28 eV), the photoinduced electrons under visible irradiation tend to transfer from the CB of g-C_3N_4 to CB of TiO_2.

Based on above calculation and analysis, an energy band structure has been proposed in Scheme 1. The photogenerated electrons and holes are unable to migrate from g-C_3N_4 to Bi_2O_3 through TiO_2. Besides, the Bi_2O_3 and g-CN_4 quantum dots don't interact and they are located in different position of TiO_2 surface. Consequently, it's believed that there are just two heterojunctions (TiO_2/g-C_3N_4, TiO_2/Bi_2O_3) instead of a ternary heterojunction.

According to the previous researches, there are three types of radical degradation mechanism, including superoxide radical ($\cdot O_2^-$), hydroxyl radical ($\cdot OH$) and hole (h^+).[3,7,8,44,45] Steps of generation of the three radicals can be explained as follows:

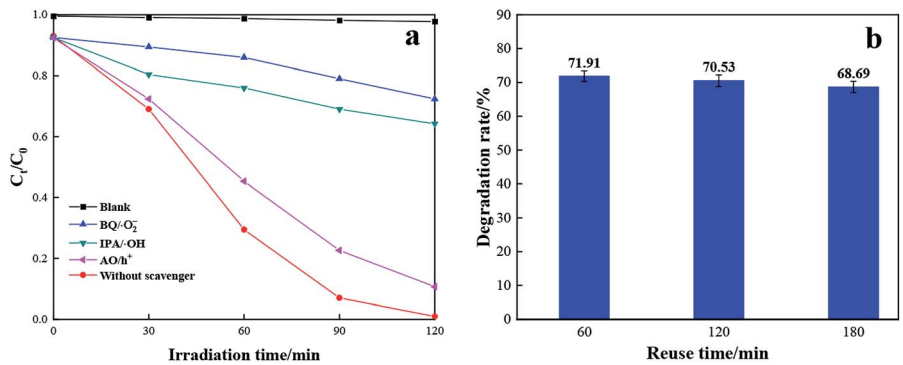

Fig. 9 Radical capture test (a) and stability test of TCB-30% for degradation of RhB (b) under sunlight irradiation.

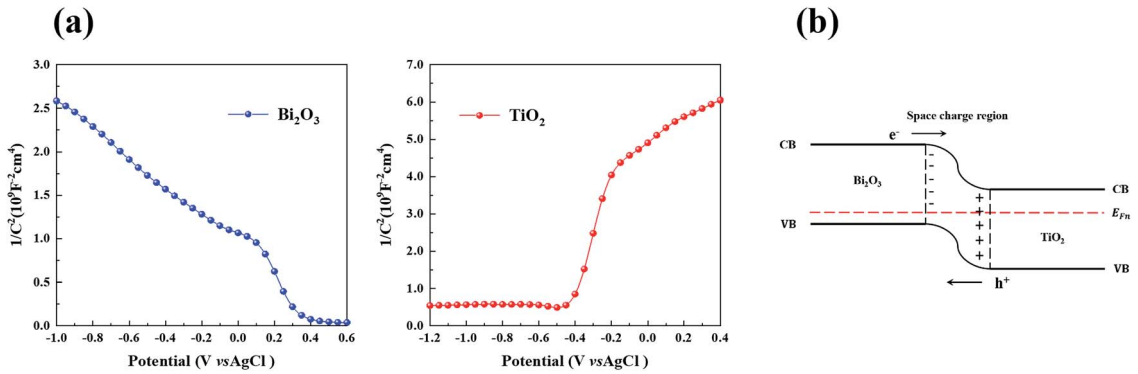

Fig. 10 (a) Mott–Schottky plots of Bi_2O_3 and TiO_2 in 0.5 M Na_2SO_4 at a frequency of 1 kHz, and (b) energy band structure of p-type Bi_2O_3/n-type TiO_2.

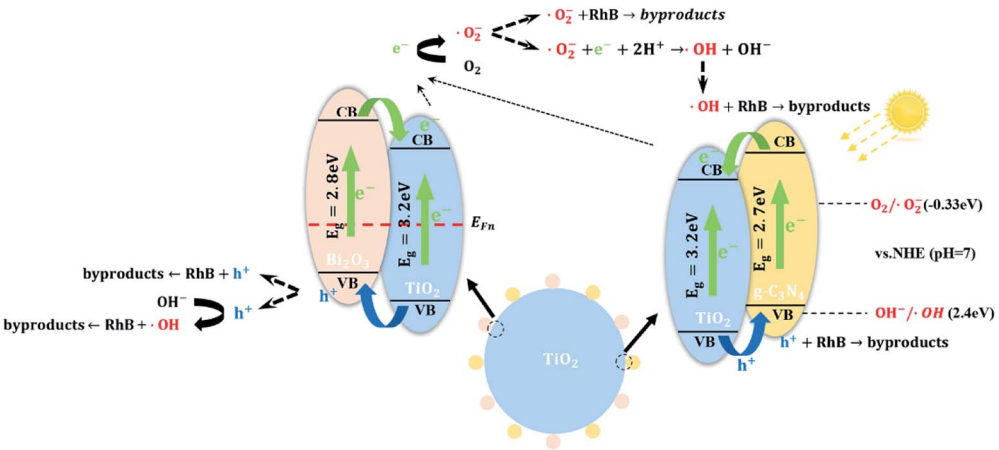

Scheme 1 Photocatalytic degradation mechanism from the generation of photoinduced electron–hole to the decomposition of dyes.

$$e^- + O_2 \rightarrow \cdot O_2^-$$

$$\cdot O_2^- + H^+ \rightarrow HO_2^{\cdot}$$

$$2HO_2 \rightarrow O_2 + H_2O_2$$

$$H_2O_2 + \cdot O_2^- \rightarrow \cdot OH + OH^- + O_2$$

$$OH^- + h^+ \rightarrow \cdot OH$$

In this work, there was a minor change in degradation performance after eliminating the holes through the scavenging test. Thus, it was concluded that the majority dye was degraded by superoxide radical ($\cdot O_2^-$) or hydroxyl radical ($\cdot OH$) induced by photo catalysis. Meanwhile, a slight number of dyes is degraded by hydroxyl radical ($\cdot OH$) induced by photoinduced holes or directly oxidation by the holes.

Eventually, the systematic mechanism, including the generation and transfer of carriers, generation of radicals and reaction between radicals and dyes, was proposed in Scheme 1.

4 Conclusion

In summary, a facile ball-milling/calcination was successively utilized to prepared a Bi_2O_3 and g-C_3N_4 quantum dots modified anatase TiO_2 heterojunction system. It was found that TCB-30% exhibited the highest removal rate for degradation of dyes under UV light irradiation and sunlight irradiation. Under sunlight irradiation, there was remarkable improvement of TCB-30%, the reaction rate constant was about 4.2 times and 3.3 times higher than that of TiO_2 and g-C_3N_4 towards degradation of RhB. The notable enhancement of photocatalytic activity is mainly due to the ability of visible light harvesting and efficient separation of the carriers, which was induced by the modification of Bi_2O_3 and g-C_3N_4 quantum dots.

Conflicts of interest

There are no conflicts to declare.

Acknowledgements

This work was supported by National Key Research and Development Program (2018YFC1802605), Nature Science Foundation of Sichuan Province (2017GZ0383, 2017SZ0181), Science Foundation of China (31100374), the Key Research and Development Project of Sichuan Province (2018GZ0455), and the Scitech innovation seedling project from Sichuan Institute of Computer Science (18-YCG041).

References

1 K. Nakata and A. Fujishima, TiO_2 photocatalysis: design and applications, *J. Photochem. Photobiol., C*, 2012, **13**(3), 169–189.

2 A. Fujishima and K. Honda, Electrochemical Photolysis of Water at a Semiconductor Electrode, *Nature*, 1972, **238**(5358), 37–38.

3 H. Dong, G. Zeng, L. Tang, C. Fan, C. Zhang, X. He and Y. He, An overview on limitations of TiO_2-based particles for photocatalytic degradation of organic pollutants and the corresponding countermeasures, *Water Res.*, 2015, **79**, 128–146.

4 V. Etacheri, C. Di Valentin, J. Schneider, D. Bahnemann and S. C. Pillai, Visible-light activation of TiO_2 photocatalysts: advances in theory and experiments, *J. Photochem. Photobiol., C*, 2015, **25**, 1–29.

5 A. Fujishima, X. Zhang and D. A. Tryk, TiO_2 photocatalysis and related surface phenomena, *Surf. Sci. Rep.*, 2008, **63**(12), 515–582.

6 Y. Ren, Y. Dong, Y. Feng and J. Xu, Compositing Two-Dimensional Materials with TiO_2 for Photocatalysis, *Catalysts*, 2018, **8**(12), 590.

7 J. Schneider, M. Matsuoka, M. Takeuchi, J. Zhang, Y. Horiuchi, M. Anpo and D. W. Bahnemann, Understanding TiO_2 Photocatalysis: Mechanisms and Materials, *Chem. Rev.*, 2014, **114**(19), 9919–9986.

8 S. G. Kumar and L. G. Devi, Review on Modified TiO_2 Photocatalysis under UV/Visible Light: Selected Results and Related Mechanisms on Interfacial Charge Carrier Transfer Dynamics, *J. Phys. Chem. A*, 2011, **115**(46), 13211–13241.

9 S. C. Yan, Z. S. Li and Z. G. Zou, Photodegradation Performance of g-C_3N_4 Fabricated by Directly Heating Melamine, *Langmuir*, 2009, **25**(17), 10397–10401.

10 J. G. Yu, S. H. Wang, J. X. Low and W. Xiao, Enhanced photocatalytic performance of direct Z-scheme g-C_3N_4-TiO_2 photocatalysts for the decomposition of formaldehyde in air, *Phys. Chem. Chem. Phys.*, 2013, **15**(39), 16883–16890.

11 J. Y. Lei, Y. Chen, F. Shen, L. Z. Wang, Y. D. Liu and J. L. Zhang, Surface modification of TiO_2 with g-C_3N_4 for enhanced UV and visible photocatalytic activity, *J. Alloys Compd.*, 2015, **631**, 328–334.

12 C. Miranda, H. Mansilla, J. Yanez, S. Obregon and G. Colon, Improved photocatalytic activity of g-C_3N_4/TiO_2 composites prepared by a simple impregnation method, *J. Photochem. Photobiol., A*, 2013, **253**, 16–21.

13 H. Li, L. Zhou, L. Wang, Y. Liu, J. Lei and J. Zhang, In situ growth of TiO_2 nanocrystals on g-C_3N_4 for enhanced photocatalytic performance, *Phys. Chem. Chem. Phys.*, 2015, **17**(26), 17406–17412.

14 Y. M. Wu, L. Tao, J. Zhao, X. Yue, W. Y. Deng, Y. X. Li and C. Y. Wang, TiO_2/g-C_3N_4 nanosheets hybrid photocatalyst with enhanced photocatalytic activity under visible light irradiation, *Res. Chem. Intermed.*, 2016, **42**(4), 3609–3624.

15 S. Bagwasi, Y. Niu, M. Nasir, B. Tian and J. Zhang, The study of visible light active bismuth modified nitrogen doped titanium dioxide photocatlysts: role of bismuth, *Appl. Surf. Sci.*, 2013, **264**, 139–147.

16 V. L. Chandraboss, J. Kamalakkannan and S. Senthilvelan, Synthesis of activated charcoal supported Bi-doped TiO_2 nanocomposite under solar light irradiation for enhanced photocatalytic activity, *Appl. Surf. Sci.*, 2016, **387**, 944–956.

17 Y. Wang, Y. Wang, Y. Meng, H. Ding, Y. Shan, X. Zhao and X. Tang, A highly efficient visible-light-activated photocatalyst based on bismuth- and sulfur-codoped TiO_2, *J. Phys. Chem. C*, 2008, **112**(17), 6620–6626.

18 Y. Wu, G. Lu and S. Li, The Doping Effect of Bi on TiO_2 for Photocatalytic Hydrogen Generation and Photodecolorization of Rhodamine B, *J. Phys. Chem. C*, 2009, **113**(22), 9950–9955.

19 D. Y. Li, Y. G. Zhang, Y. L. Zhang, X. F. Zhou and S. J. Guo, Fabrication of bidirectionally doped beta-Bi_2O_3/TiO_2-NTs with enhanced photocatalysis under visible light irradiation, *J. Hazard. Mater.*, 2013, **258**, 42–49.

20 Y. Bessekhouad, D. Robert and J. V. Weber, Photocatalytic activity of CU_2O/TiO_2, Bi_2O_3/TiO_2 and $ZnMn_2O_4$/TiO_2 heterojunctions, *Catal. Today*, 2005, **101**(3–4), 315–321.

21 Z. F. Bian, J. Zhu, S. H. Wang, Y. Cao, X. F. Qian and H. X. Li, Self-assembly of active Bi_2O_3/TiO_2 visible photocatalyst with ordered mesoporous structure and highly crystallized anatase, *J. Phys. Chem. C*, 2008, **112**(16), 6258–6262.

22 Y. D. Liu, F. Xin, F. M. Wang, S. X. Luo and X. H. Yin, Synthesis, characterization, and activities of visible light-driven Bi_2O_3-TiO_2 composite photocatalysts, *J. Alloys Compd.*, 2010, **498**(2), 179–184.

23 J. Hou, C. Yang, Z. Wang, S. Jiao and H. Zhu, Bi_2O_3 quantum dots decorated anatase TiO_2 nanocrystals with exposed {001} facets on graphene sheets for enhanced visible-light photocatalytic performance, *Appl. Catal., B*, 2013, **129**, 333–341.

24 Y. Liu, F. Xin, F. Wang, S. Luo and X. Yin, Synthesis, characterization, and activities of visible light-driven Bi_2O_3-TiO_2 composite photocatalysts, *J. Alloys Compd.*, 2010, **498**(2), 179–184.

25 S. Sood, S. K. Mehta, A. S. K. Sinha and S. K. Kansal, Bi_2O_3/TiO_2 heterostructures: synthesis, characterization and their application in solar light mediated photocatalyzed degradation of an antibiotic, ofloxacin, *Chem. Eng. J.*, 2016, **290**, 45–52.

26 J. Xu, Y. Ao, D. Fu and C. Yuan, Synthesis of Bi_2O_3-TiO_2 composite film with high-photocatalytic activity under sunlight irradiation, *Appl. Surf. Sci.*, 2008, **255**(5), 2365–2369.

27 Y. Zhang, J. Lu, M. R. Hoffmann, Q. Wang, Y. Cong, Q. Wang and H. Jin, Synthesis of g-C_3N_4/Bi_2O_3/TiO_2 composite nanotubes: enhanced activity under visible light irradiation and improved photoelectrochemical activity, *RSC Adv.*, 2015, **5**(60), 48983–48991.

28 Z. Zhao, J. Tian, D. Wang, X. Kang, Y. Sang, H. Liu, J. Wang, S. Chen, R. I. Boughton and H. Jiang, UV-visible-light-activated photocatalysts based on Bi_2O_3/$Bi_4Ti_3O_{12}$/TiO_2 double-heterostructured TiO_2 nanobelts, *J. Mater. Chem.*, 2012, **22**(44), 23395–23403.

29 J. Guo, J. Liang, X. Yuan, L. Jiang, G. Zeng, H. Yu and J. Zhang, Efficient Visible-Light Driven Photocatalyst, Silver (meta)vanadate: Synthesis, Morphology and Modification, *Chem. Eng. J.*, 2018, **352**, 782–802.

30 Mi-H. Jung and M. Gu Kang, Enhanced photo-conversion efficiency of CdSe–ZnS core–shell quantum dots with Au nanoparticles on TiO_2 electrodes, *J. Mater. Chem.*, 2011, **21**, 2694.

31 J. Hou, C. Yang, Z. Wang, S. Jiao and H. Zhu, Bi_2O_3 quantum dots decorated anatase TiO_2 nanocrystals with exposed {001} facets on graphene sheets for enhanced visible-light photocatalytic performance, *Appl. Catal., B*, 2013, **129**, 333–341.

32 G. Lia, Z. Liana, W. Wanga, D. Zhanga and H. Lia, Nanotube-confinement induced size-controllable g-C_3N_4 quantum dots modified single-crystalline TiO_2 nanotube arrays for stable synergetic photoelectrocatalysis, *Nano Energy*, 2016, **19**, 446–454.

33 W.-K. Jo, T. Adinaveen, J. J. Vijaya and N. C. S. Selvam, Synthesis of MoS_2 nanosheet supported Z-scheme TiO_2/g-C_3N_4 photocatalysts for the enhanced photocatalytic degradation of organic water pollutants, *RSC Adv.*, 2016, **6**(13), 10487–10497.

34 B. Naik, S. Martha and K. M. Parida, Facile fabrication of Bi_2O_3/$TiO_{2-x}N^x$ nanocomposites for excellent visible light driven photocatalytic hydrogen evolution, *Int. J. Hydrogen Energy*, 2011, **36**(4), 2794–2802.

35 M. SGe, C. Cao, S. Li, S. Zhang, S. Deng, J. Huang, Q. Li, K. Zhang, S. S. Al-Deyab and Y. Lai, Enhanced photocatalytic performances of n-TiO_2 nanotubes by uniform creation of p–n heterojunctions with p-Bi_2O_3 quantum dots, *Nanoscale*, 2015, **7**(27), 11552–11560.

36 Z. Lu, L. Zeng, W. Song, Z. Qin, D. Zeng and C. Xie, In situ synthesis of C-TiO_2/g-C_3N_4 heterojunction nanocomposite as highly visible light active photocatalyst originated from effective interfacial charge transfer, *Appl. Catal., B*, 2017, **202**, 489–499.

37 G. Dong, Y. Zhang, Q. Pan and J. Qiu, A fantastic graphitic carbon nitride (g-C_3N_4) material: electronic structure, photocatalytic and photoelectronic properties, *J. Photochem. Photobiol., C*, 2014, **20**, 33–50.

38 J. Fu, J. Yu, C. Jiang and B. Cheng, g-C_3N_4-Based Heterostructured Photocatalysts, *Adv. Energy Mater.*, 2018, **8**(3), 1701503.

39 W.-J. Ong, 2D/2D Graphitic Carbon Nitride (g-C_3N_4) Heterojunction Nanocomposites for Photocatalysis: Why Does Face-to-Face Interface Matter?, *Front. Mater. Sci.*, 2017, **4**, DOI: 10.3389/fmats.2017.00011.

40 Y. Wu, L. Tao, J. Zhao, X. Yue, W. Deng, Y. Li and C. Wang, TiO_2/g-C_3N_4 nanosheets hybrid photocatalyst with enhanced photocatalytic activity under visible light irradiation, *Res. Chem. Intermed.*, 2016, **42**(4), 3609–3624.

41 H. Yan and H. Yang, TiO_2-g-C_3N_4 composite materials for photocatalytic H-2 evolution under visible light irradiation, *J. Alloys Compd.*, 2011, **509**(4), L26–L29.

42 N. Yang, G. Li, W. Wang, X. Yang and W. F. Zhang, Photophysical and enhanced daylight photocatalytic properties of N-doped TiO_2/g-C_3N_4 composites, *J. Phys. Chem. Solids*, 2011, **72**(11), 1319–1324.

43 K. Li, S. Gao, Q. Wang, H. Xu, Z. Wang, B. Huang, Y. Dai and J. Lu, In-Situ-Reduced Synthesis of Ti^{3+} Self-Doped TiO_2/g-C_3N_4 Heterojunctions with High Photocatalytic Performance under LED Light Irradiation, *ACS Appl. Mater. Interfaces*, 2015, **7**(17), 9023–9030.

44 M. A. M. Adnan, N. M. Julkapli, M. N. I. Amir and A. Maamor, Effect on different TiO_2 photocatalyst supports on photodecolorization of synthetic dyes: a review, *Int. J. Environ. Sci. Technol.*, 2019, **16**(1), 547–566.

45 P. Huo, P. Kumar and B. Liu, The Mechanism of Adsorption, Diffusion, and Photocatalytic Reaction of Organic Molecules on TiO_2 Revealed by Means of On-Site Scanning Tunneling Microscopy Observations, *Catalysts*, 2018, **8**(12), 616.